Advances in Water Resources 32 (2009) 1187–1196

Contents lists available at ScienceDirect

Advances in Water Resources

journal homepage: www.elsevier.com/locate/advwatres

A two-phase numerical model for suspended-sediment transport in estuaries

Kim Dan Nguyen [a,d], Sylvain Guillou [b,*], Julien Chauchat [a], Nathaly Barbry [c]

[a] Laboratory of Continental and Coastal Morphodynamics, UMR CNRS 6143, University of Caen, Campus II, F-14034 Caen Cedex, France
[b] Laboratoire Universitaire des Sciences Appliquées de Cherbourg (LUSAC) EA 2607, University of Caen, Site universitaire de Cherbourg, BP78, 50130 Cherbourg - Octeville, France
[c] Laboratoire de Génie Civil et Mécanique (GeM), UMR CNRS 6183/Université de Nantes, 58 rue Michel Ange, F-44600 Saint-Nazaire Cedex, France
[d] Saint-Venant Laboratory for Hydraulics, Joint-Research Unit of CETMEF, EDF R&D and ENPC, 6 Quai Wattier, 78400 Chatou, France

ARTICLE INFO

Article history:
Received 6 May 2008
Received in revised form 25 March 2009
Accepted 4 April 2009
Available online 14 April 2009

Keywords:
Numerical modelling
Two-phase fluid-particle modelling
Sediment transport
Estuary

ABSTRACT

This paper presents a full 2-D X/Z numerical model for sediment transport in open channels and estuaries using a two-phase (fluid–solid particle) approach. The physical concept and the mathematical background of the model are given and test-cases have been carried out to validate the proposed model. In order to illustrate its feasibility for a real estuary, the model has been applied to simulate the suspended-sediment transport and the formation of turbidity maximum in the Seine estuary. The numerical results show that the main characteristics of estuarine hydro-sediment dynamics in the Seine estuary are in fact reproduced by the proposed model. A qualitative agreement between the numerical results and the actual observations has been obtained and is presented in this paper.

1. Introduction

The main feature of fine-grained sediment transport in macro-tidal estuaries is the formation and displacement of "turbidity maximum" (TM), a phenomenon that has been well documented. The TM, characterized by a high-suspended matter concentration zone, is a trap for the most important organic, trace metal or radionuclide pollutant resources in estuaries. Sediment transport and TM modelling must therefore be carried out in advance of any environmental study.

In the last two decades, many numerical models of suspended-sediment transport in estuaries and coastal zones have been made [1–11]. Most of the existing numerical models, which are single-phase (classic at the time) are based on the hypothesis that solid particles move at the same velocity as fluid-particles, with the exception of their falling velocity. This is known as the "passive scalar" hypothesis. One important advantage of single-phase models is that they do not require significant CPU time and can provide results which may be used to solve engineering problems. However, there remain a number of flaws regarding the physical concept. The impact of particle motion upon fluid flows, for example, is ignored. Nor are particle–particle interactions, which can be very strong in dense flows, taken into account. Another problem arises from the definition of the estuary beds. It is well known that near the bottom of the estuary, there is usually a layer of fluid mud, whose concentration exceeds 20–100 $g\,l^{-1}$. In this layer, processes of sedimentation (or re-suspension), of solid-particle consolidation and of bed settling occur. The bed–fluid exchange is in fact deposition and re-suspension on the surface of this layer. Since the processes of consolidation and of bed settling could not be taken into consideration in the single-phase models, a fictive bed, where the solid concentration exceeds about 100 $g\,l^{-1}$, should be introduced in order to define the computing domain of the model. The mud layer beyond this fictive bed constitutes a limited fine-grained reservoir for sediment exchanges between the fluid and the bed. Models for solid-particle Consolidation and Settling Bed (CSB) are necessary and the state of the art of such models is available in Winterwerp and Van Kesteren [12]. Single-phase models should be then coupled with CSB models in order to provide a complete model of sediment transport. The coupling is based on the balance of sediment fluxes exchanged between these two models.

The major difficulties in such a modelling are met in determining the erosion and deposition rates and the falling velocity of solid particles in fluid. The exchange between fluid and bed is evaluated through deposition and erosion fluxes crossing the fictive bed surface by several empirical formulas. Blaas et al. [1], and Gleinzon et al. [3] have separated the bed sediment into two layers – a top layer of unconsolidated sediment and a bottom layer of consolidated sediment. Gleinzon et al. [3] use the formula for the erosion rate proposed by Mehta et al. [13] for soft unconsolidated sediment and by Ariathurai and Arulanandan [14]

* Corresponding author.
E-mail addresses: nguyen@unicaen.fr (K.D. Nguyen), sylvain.guillou@unicaen.fr (S. Guillou), julien.chauchat@unicaen.fr (J. Chauchat), nathaly.barbry@univ-nantes.fr (N. Barbry).

0309-1708/$ - see front matter © 2009 Elsevier Ltd. All rights reserved.
doi:10.1016/j.advwatres.2009.04.001

for hard, consolidated sediment. Also [14] has been used in Blass et al. [1], Li et al. [4], Nguyen et al. [9]. The formula for the erosion rate proposed by Partheniades [15] has been used in Liu et al. [5], Lumborg [7], Lumborg and Pejrup [8], and the one proposed by Hayter and Mehta [16] has been used in Lopes et al. [6]. As far as the deposition rate is concerned, the formula proposed by Krone [17] is used in most of the existing modellings. In these empirical formulas, many parameters must be defined *a priori* by users. These parameters depend on geological conditions such as bed materials and on the degree of bed consolidation – data that is often incomplete or even absent altogether. Only a sufficient number of field surveys would allow us to calibrate the model by tuning these empirical parameters. And only after (at least) one serious calibration and some verification, could the model provide accurate simulations. However, these simulations would only be correct in the specific conditions close enough to those of the calibration and verification. Consequently, the single-phase models are likely to lose predictive capacity and eventually, their utility. In order to correct the flaws mentioned above, another approach, which consists of studying the flows in two-phase – flows (fluid and solid particles), has been developed.

In a two-phase sediment transport model, the computing domain is extended to the "true" non-erodible bottom, while the governing equations are the same for both high and low concentration areas of the domain. Fluid flows are free surface and considered as non-hydrostatic. The main physical processes for sediment transport such as fluid–solid particles, particle–particle interactions, particle–wall collision, and fluid-bottom exchanges are integrated into the equations of motion and treated as momentum exchanges between phases. The fluid mud is handled as a non-Newtonian fluid. In the physical sense, this approach is more complex, but more realistic than the single-phase modelling.

There are very few two-phase models for sediment transport in existence. Teisson et al. [18] were the first to propose a quasi 1-D vertical, two-phase model, based on the work done by Simonin [19]. In this model, horizontal gradients are nil, except for the pressure gradient, which is imposed as an external force. Fluid and solid particles thus move at the same horizontal velocity. Vilaret and Davies [20] present a comparison between the classic, single-phase model and Teisson et al.'s model, focusing on fluid and non-cohesive particle interaction. The authors show the value of the two-phase approach in describing the physical process of suspended-sediment transport, especially in the mud layer near the bottom. Greimann and Holly [21] used the two-phase flow equation to develop relations for the vertical profiles of concentrations in an open-channel and for uniform flow over a flat sediment-starved bed with single-sized sediment in suspension. In Barbry et al. [22], a brief presentation of a 2-D two-phase flow model for estuaries is given. The technique for determining the free surface level in non-hydrostatic flows initially proposed by Guillou et al. [23] has been used in this model. Some test-cases are then presented to qualitatively validate the model. However, as the authors show, developments of the model have not yet progressed beyond the preliminary stages.

The purpose of this article is therefore to present the fully improved 2-D X/Z model for the suspended-sediment transport in variable-width channels and estuaries using the two-phase (fluid and solid particle) approach. Section 2 briefly presents the mathematical and numerical background of the model. Several test-cases which validate the current model are given in Section 3. Some results of the application of the model to the Seine estuary (France) are presented in Section 4 as an illustration of the feasibility of the model. Section 5 explores the prospects for developing and improving two-phase models of sediment transport.

2. Description of the two-phase flow model

2.1. Mathematical background

In an Eulerian formulation, the averaged governing equations for the k-phase are provided by Drew and Lahey [25]. In the particular case of a 2-D XZ model a width-integrated set of equations can be written (continuity and momentum equations):

$$\begin{cases} \frac{\partial(\alpha_k B)}{\partial t} + \vec{\nabla}\cdot(\alpha_k B\,\vec{u_k}) = 0 \\ \frac{\partial(\alpha_k \vec{u_k})}{\partial t} + \vec{\nabla}\cdot(\alpha_k \rho_k \vec{u_k}\otimes\vec{u_k}) \\ \quad = \frac{1}{B\rho_k}\vec{\nabla}\cdot\left(\alpha_k B\left(-p_k\bar{\bar{I}} + \overline{\overline{\tau_k}} + \overline{\overline{\tau_k^{Re}}}\right)\right) + \alpha_k\vec{g} + \frac{1}{B\rho_k}\vec{M_k} \end{cases} \quad (1)$$

where α_k represents the volume fraction of the k-phase, with $\alpha_s + \alpha_f = 1$, ρ_k is the averaged density, B is the width of the estuary or the channel and $\vec{u}_k$ is the averaged velocity vector of k-phase. k is "f" for the fluid phase and "s" for the solid phase. $\vec{g}$ is the gravity acceleration and $\vec{M}_k$ is the momentum exchanged between these two phases. p_k is the pressure, $\overline{\overline{\tau_k}}$ is the shear stress tensor and $\overline{\overline{\tau_k^{Re}}}$ is the turbulent Reynolds stress tensor for k-phase.

In the present work the fluid turbulence is addressed using a simple zero equation model in which the influence of sediments on the turbulence is neglected. Due to the complexity of two-phase models, fluid-particles turbulent interactions and two-phase turbulence modelling are beyond the scope of this paper, but readers can find *details concerning this point* in Chauchat and Guillou [24].

The viscous shear stress of the fluid depends on the strains of the fluid and of the solid. They are determined on the base of the model proposed by Lundgren [26]:

$$\alpha_f\overline{\overline{\tau_f}} = \mu_{fs}\overline{\overline{D_s}} + \mu_{ff}\overline{\overline{D_f}} \quad \alpha_s\overline{\overline{\tau_s}} = \mu_{ss}\overline{\overline{D_s}} + \mu_{sf}\overline{\overline{D_f}} \quad (2)$$

In that relation $\overline{\overline{D_f}}$ and $\overline{\overline{D_s}}$ are the strain tensors of the fluid and solid phases given by:

$$\overline{\overline{D_f}} = \frac{1}{2B}\left[\vec{\nabla}B\,\vec{u_f} + {}^t\left(\vec{\nabla}B\,\vec{u_f}\right)\right] \quad \text{and} \quad \overline{\overline{D_s}} = \frac{1}{2B}\left[\vec{\nabla}B\,\vec{u_s} + {}^t\left(\vec{\nabla}B\,\vec{u_s}\right)\right] \quad (3)$$

The coefficients for the fluid are related to the viscosity of the fluid by (4), whereas the coefficients for the solid are related to the viscous effect of the particle taken into account by the introduction of the coefficient β in (5). Thus the non-Newtonian properties of the solid-particle phase are taken into account.

$$\mu_{ff} = \alpha_f\mu_f \quad \mu_{fs} = \alpha_s\mu_f \quad (4)$$

$$\mu_{ss} = \alpha_s\beta\mu_{fs} \quad \mu_{sf} = \alpha_s\beta\mu_{ff} \quad (5)$$

μ_{ff}, μ_{fs}, μ_{sf} and μ_{ss} designate viscosity effective coefficients, which are proportional to the viscosity of fluid, μ_f. β is the amplification factor of viscous stresses and depends on ξ – the distance between solid particles. It is introduced to take the particle–particle interaction into consideration. Following Einstein's formula [27], $\beta = 5/2$ for diluted suspensions, $\alpha_s < 0.03$. In estuaries and coastal zones, sediment concentration can (and usually does) vary from very dilute to extremely dense in turbidity maximum. A theoretical model, which covers all of the cases met in nature, from diluted suspensions to compacted particulate layers was presented by Graham [28]:

$$\beta = \frac{5}{2} + \frac{9}{4}\left(\frac{1}{1+\xi/d}\right)\left[\frac{1}{2\xi/d} - \frac{1}{1+2\xi/d} - \frac{1}{(1+2\xi/d)^2}\right]\frac{1}{\alpha_s} \quad (6)$$

where ξ is the inter-distance between nearby solid particles and d is the size of solid particles. Ratio ξ/d is given by:

$$\xi/d = \frac{1-(\alpha_s/\alpha_{s,\max})^{1/3}}{(\alpha_s/\alpha_{s,\max})^{1/3}} \tag{7}$$

where $\alpha_{s,\max}$ is equivalent to the maximum value of the solid-particle concentration, which must be experimentally determined. For rigid spheres, $\alpha_{s,\max}$ is usually taken as equal to 0.625. It must be noted that, $\alpha_{s,\max}$-value can greatly affect numerical results.

Enwald et al. [29] show that the "pressure" in a particulate phase, p_s, is the result of a combination of three effects: the first one, $p_{s,cin}$, corresponds to the transport momentum engendered by the fluctuation of the solid-particle velocity. The second one, $p_{s,coll}$, is due to particle–particle interaction (collision). The latter, p_f, represents the contribution of the fluid pressure. Because the kinetic pressure is often negligible, the pressure gradient of the solid-particle phase is written by (8).

$$\vec{\nabla}(\alpha_s p_s) = \vec{\nabla}(\alpha_s p_{s,coll}) + \vec{\nabla}(\alpha_s p_f) \tag{8}$$

$$\vec{\nabla}(\alpha_s p_{s,coll}) = -G(\alpha_f)\vec{\nabla}\alpha_s \tag{9}$$

The first term of RHS of (8) is the solid pressure gradients collision effects. The last term represents the buoyancy effect, i.e. the solid-particle pressure can be increased or decreased, depending on the sign of the fluid pressure gradient. The pressure gradient by collision is determined by (9). The term $\vec{\nabla}(\alpha_s p_{s,coll})$, which refers to the force of particle–particle interaction, keeps solid particles separated from one another, so that the particle phase does not become too dense and compacted. $G(\alpha_f)$ is equivalent to the elastic module of the solid-particle phase and is modelled empirically. Massoudi et al. [30] proposed two models for $G(\alpha_f)$:

$$G(\alpha_f) = G_0 e^{-C(\alpha_f-\alpha^*)} \quad \text{and} \quad G(\alpha_f) = 10^{B_1\alpha_f+B_2} \tag{10}$$

Constants B_1, B_2, G_0, C and α^* are empirically determined and given by Enwald et al. [29]. Eqs. (9) and (10) take into consideration the collisions between solid particles. This phenomenon has the effect of hindering the process of sedimentation.

The transfer laws, describing the interactions between the phases are given by:

$$\begin{aligned}\vec{M}_f &= p_{fi}\vec{\nabla}\alpha_f - \overline{\overline{\tau_{fi}}}\vec{\nabla}\alpha_f + \vec{M}'_f\\ \vec{M}_s &= p_{si}\vec{\nabla}\alpha_s - \overline{\overline{\tau_{si}}}\vec{\nabla}\alpha_s + \vec{M}'_s\end{aligned} \tag{11}$$

where $\vec{M}'_f = -\vec{M}'_s$, which will be detailed below; p_{ki} and $\overline{\overline{\tau_{ki}}}$ are the pressure and the shear–stress tensor of k-phase at the interface. The fluid pressure at the interface is determined by Bernoulli's equation as follows:

$$p_{fi} = p_f - \frac{\rho_f}{4}\left\|\vec{u_f} - \vec{u_s}\right\|^2 \tag{12}$$

Because of constant temperature, the classic Laplace equation gives the following relationship between p_{si} and p_{fi}:

$$p_{si} = p_{fi}. \tag{13}$$

The shear–stress tensor of the fluid and solid-particle phases at the interface is calculated by:

$$\overline{\overline{\tau_{si}}} = \overline{\overline{\tau_{fi}}} = \beta\overline{\overline{\tau_f}} \tag{14}$$

The momentum exchanged between two-phases $\vec{M}'_s = -\vec{M}'_f$ is the sum of the forces exerted on the solid particles: the virtual mass force, the lift force, the Faxén force, the Basset force and the drag force. In estuarine and coastal flows, the drag force is dominant, and hence the only one to be retained is the drag force Hsu et al. [37], Guillou and Chauchat [24]. Then, the momentum exchanged is written as:

$$\vec{M}'_s \approx \vec{F}_D = \frac{\alpha_s\rho_s}{\tau_{fs}}\vec{u}_r \tag{15}$$

where $\vec{u}_r$ is the relative velocity of fluid-particles, and τ_{fs} is the particle relaxation time, which represents the entrainment of the particles by the fluid phase. The relative velocity of fluid-particles is defined as $\vec{u}_r = \vec{u}_s - \vec{u}_f - \vec{u}_d$. The drift velocity $\vec{u}_d = \langle\vec{u}'_f\rangle_s$ represents the correlation between the fluctuating velocity of the fluid phase and the instantaneous spatial distribution of the solid-particle phase (Peirano and Leckner [31], Deutch and Simonin [32]). As the flow is laminar it is not considered here. τ_{fs} is defined by:

$$\tau_{fs} = \frac{4d\rho_s}{3\rho_f C_D\|\vec{u}_r\|} \tag{16}$$

In that relation, $C_D = \frac{24}{Re_s}f(Re_s,\psi)$ is the averaged drag coefficient, depending on the Reynolds number $Re_s = \frac{d\|\vec{u}_r\|}{\nu_f(1+\alpha_s\beta)}$, and on the solid-particle shape Ψ. In cases where $Re_s < 1$, $f = 1$, then the coefficient C_D retains Stokes' formula. Some formulas for function $f(Re_s,\psi)$ when Re_s increases do exist. More recently, Haider and Levenspiel [33] have proposed a formula for $Re_s < 25 \times 10^3$:

$$C_D = \frac{24}{Re_s}\left[1 + e^{2.3288-6.4581\psi^2 Re_s^{0.0964+0.5565\psi}}\right] + \frac{Re_s e^{4.905-13.8944\psi+18.4222\psi^2-10.2599\psi^2}}{Re_s + e^{1.4681-12.2584\psi+20.7322\psi^2+15.8855\psi^2}} \tag{17}$$

As Re_s varies, in estuaries, from 10^{-6} for clays to $4\cdot10^2$ for coarse sands. Therefore, (17) is the most suitable for suspended-sediment transport modelling.

2.2. Numerical techniques

The application of the model to estuaries and coastal zones, where tidal range and bathymetrical variations are very large, needs an adaptative Eulerian grid in a sigma co-ordinate system. This technique perfectly fits the first and last grid lines into the bottom and the water surface, respectively (Fig. 1). A co-ordinate transformation from the Cartesian co-ordinate system (x, z, t) into the sigma system (x^*, σ, t^*) is done as follows:

$$x^* = x; \quad \sigma = \frac{z+h}{\eta+h} = \frac{z+h}{H}; \quad t^* = t \tag{18}$$

where x is the longitudinal co-ordinate; z is the ascending vertical co-ordinate; η is the water surface level; h is the bottom depth and $H = \eta + h$ is the total water depth.

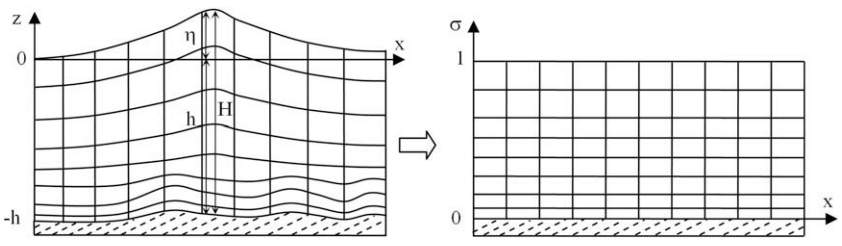

Fig. 1. Co-ordinate system transformation: physical plan (left) and computational plan (right).

Obviously, σ varies from 0 to 1 when z varies from $-h$ to η. Let us now consider a scalar variable, $\phi(x,z,t) = \phi(x^*,\sigma,t^*)$. The relationship between the ϕ-derivates of two co-ordinate systems is given as follows:

$$\begin{cases} \dfrac{\partial\phi}{\partial x} = \dfrac{\partial\phi}{\partial x^*} + \dfrac{1}{H}\left(\dfrac{\partial h}{\partial x^*} - \sigma\dfrac{\partial H}{\partial x^*}\right)\dfrac{\partial\phi}{\partial\sigma} \\ \dfrac{\partial\phi}{\partial z} = \dfrac{1}{H}\dfrac{\partial\phi}{\partial\sigma} \\ \dfrac{\partial\phi}{\partial t} = \dfrac{\partial\phi}{\partial t^*} - \dfrac{1}{H}\sigma\dfrac{\partial\eta}{\partial t^*}\dfrac{\partial\phi}{\partial\sigma} \end{cases} \tag{19}$$

The application of (19) to equations of system (1), which are projected in x and z directions, yields the continuity and momentum equations for the fluid phase (A.1)–(A.3), and for the solid-particle phase (A.4)–(A.6) which may be found in the Appendix of this document.

Chorin's projection method [34] is applied to calculate the pressure p_f and the velocity $\vec{u}_f$ for the fluid phase as Guillou et al. [23]. To prevent the appearance of spurious oscillations on the pressure for such a method [35] a staggered grid is used in conjunction with the finite-difference technique. Eqs. (A.1)–(A.3) are then solved in three steps: convection–diffusion, pressure and velocity-correction. In the convection–diffusion step, Eq. (A.8) is solved using a hybrid or TVD 2nd order scheme for convection and diffusion terms, an explicit scheme in x-direction and an implicit scheme in z-direction. The combination of the equations in (A.9) yields a Poisson-type equation (A.10) for a single unknown variable, p_f. The pressure terms are then discretised by a centered, and then a 2nd scheme. The GMRES (Generalised Minimal RESidual) method is then used to solve the linear equation system that results from the discretising equation (A.10). At the new time step, as the water surface level η is not yet known and the pressure distribution is non-hydrostatic, an iterative procedure should be integrated into the model in order to determine the water surface elevation and the fluid pressure with respect to the cinematic and dynamic conditions at the free surface (A.7a) and (A.7b). When the new values of the fluid pressure and the water surface level are known, Eq. (A.9) may be used for the velocity-correction step to up-date the velocity values.

Once the pressure and velocity fields are known for the fluid phase at the new time step, the solid-particle velocity vector, $\vec{u}_s$, can be determined from the momentum equation (A.5) and (A.6), by the same method that is used for determining $\vec{u}_f$, and then the volume fraction, α_s, can be calculated from the continuity equation (A.4). Our experiences show that in order to insure the convergence of numerical result of a two-phase problem, the mass conservation should be strictly respected. Therefore, the continuity equation for the solid phase (A.4) is written in the conservative form and solved using a finite volume method. The volume fraction for fluid, α_f, can be then obtained using the relationship $\alpha_f = 1 - \alpha_s$.

The procedure of calculation for a time step is as follows:

(1) Initialising the variable values p_f, $\vec{u}_f$, α_f, $\vec{u}_s$, α_s and η at $t = t_n$.
(2) Determining η the boundary conditions on the surface (A.7a) and (A.7b).
(3) Calculating $\vec{u}_f$ in the convection–diffusion step when solving (A.8).
(4) Determining p_f by iteration at $t = t_{n+1}$ using (A.10).
(5) Correcting the fluid velocity by (A.9) with the new values of η and p_f.
(6) Determining α_s by solving equation (A.4) and then deducing $\alpha_f = 1 - \alpha_s$.
(7) Calculating $\vec{u}_s$ and p_s using (A.5) and (A.6).
(8) Test of convergence $|\phi^{m+1} - \phi^m| \leqslant \varepsilon$, where ϕ may be the pressure, the velocity components and the volume faction of each phase; ε is a tolerant value and m is the index of iteration step; if the convergence is still not reached, return to step 2.
(9) Ending the time step $t = t_{n+1}$ if the convergence criteria are satisfied. In general, 2–3 iterations are sufficient to reach the convergence.

Clearly the above-cited iteration procedure insures a coupling between the two phases even in a time step.

3. Validations

3.1. Sedimentation of polystyrene particles in a still fluid

This section presents a quantitative test-case. Let us consider the sedimentation of suspended polystyrene particles (diameters of 290 ± 30 μm, density of 1.05 kg m^{-3}), falling through a tank of silicon oil (viscosity of 20 m Pa s^{-1}, density of 0.95 kg m^{-3}). Pham Van Bang et al. [36], using Magnetic Resonance Imaging (MRI), experimentally studied the evolution of particle-concentration profile in this tank. A mixing procedure was used to obtain a well-mixed fluid of uniform concentration, initially $\alpha_s = 0.48$, i.e. the mixed fluid is very dense. The profiles of polystyrene-particle concentration were averaged over 16 samples every 3 s.

The present model is employed to reproduce the sedimentation of the polystyrene particles numerically. An 11×91 grid with refinement in proximity of the bottom is then used to discretise the mixed-fluid tank of 2.5 cm width and 10 cm height. The time step is 5×10^{-4} s. The boundary conditions are also given in Table 1. $\alpha_{s,\max}$-value is fixed at 0.6 in this test-case. The maximum relative error is a minute 2×10^{-7}.

Fig. 2 presents the iso-values of the solid volume fraction, α_s at 5 min intervals. As on the experimentation of Pham Van Bang et al. [36], the numerical results show the presence of two interfaces: one that separates the clear fluid and the mixed fluid of $\alpha_s = 0.48$, and another one between the mixed fluid and the consolidated sediment of $\alpha_{s,\max} = 0.6$. The latter corresponds to a lutocline. The positions of these interfaces evolve in opposite directions, as shown in Fig. 3, in which the numerical and experimental results are compared. Evidently, there is a strong agreement between the two of them.

Fig. 4 shows the vertical profiles of the solid volume fraction obtained from the model and from Pham Van Bang et al.'s experiment, at different times. The agreement observed in this diagram confirms the capabilities of the two-phase model in modelling the sedimentation of non-cohesive solid particles in a very dense, particle-laden flow ($\alpha_s > 0.48$).

3.2. Sedimentation and consolidation of cohesive solid particles in a still water

Let us consider an experiment concerning the sedimentation of fluid mud in a tank of 1.50 m height and 0.2 m width. This

Table 1
Boundary conditions for the test-cases 3–1, 3–2 and 3–3.

	West end	East end	Bottom
H	$\frac{\partial\eta}{\partial n} = 0$	$\frac{\partial\eta}{\partial n} = 0$	
u_k	$u_k = 0$	$u_k = 0$	$u_k = 0$
w_k	$\frac{\partial w_k}{\partial n} = 0$	$\frac{\partial w_k}{\partial n} = 0$	$w_k = 0$
Φ	$\frac{\partial\phi}{\partial n} = 0$	$\frac{\partial\phi}{\partial n} = 0$	

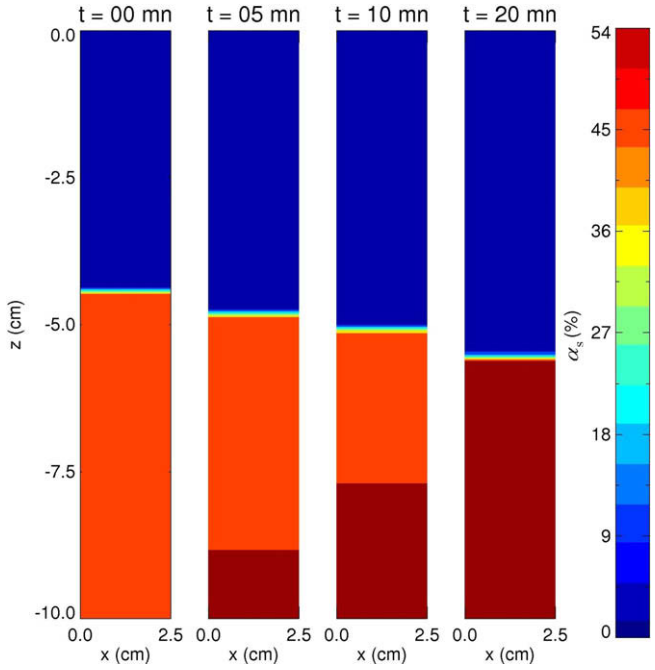

Fig. 2. Solid volume fraction field for different time. Evolution of the interface between clear fluid-mixed fluid and the lutocline.

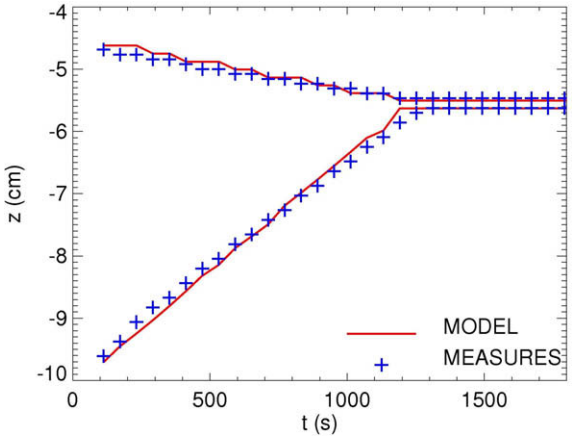

Fig. 3. Evolution over the time of the interface between the clear water and the mixture, and of the lutocline: computed (—) and experimental data (+++).

experiment is described by Rouas [38]. Initially, the solid volume fraction of the fluid mud is $\alpha_s = 0.02$ ($\rho_s = 2650\ \mathrm{kg\ m^{-1}}$) everywhere. As the flocculation process is not taken into account, this test has the ambition to show the limits of the actual assumptions. It is well known that for a mud settling test in clear water, three phases can be observed: constant rate settling; hindered settling; and consolidation (crushing of the flocs). During the second phase, the sediment concentration increases rapidly as the flocs accumulate on the bottom, and the settling velocity slows down. During the consolidation process, a continuous solid skeleton is formed and evolves under its self-weight.

Within the simulation, the diameter of solid particles is set to 20 μm. Under the effect of sedimentation, the clear water–sediment interface slowly falls during the experiment. Fig. 5 shows the evolution of the computed and measured water–sediment interface versus the time for a period of 1000 min. It should be

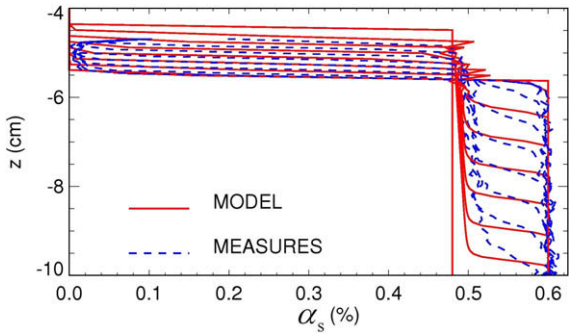

Fig. 4. The instantaneous profiles of the solid volume fraction at different times: computed (—) and measured data (- - -).

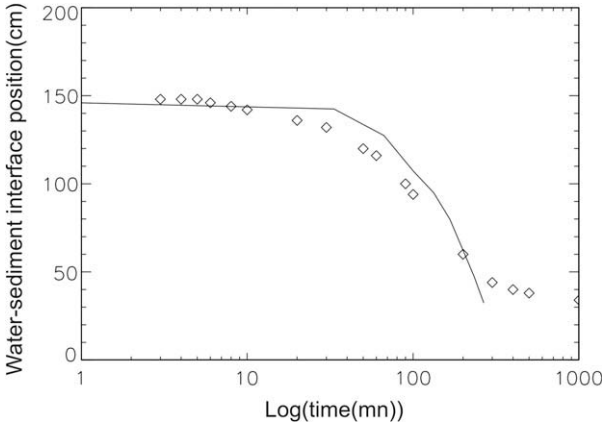

Fig. 5. Evolution of clear water–sediment interface for 1000 min: computed —; Experimental ◇.

noted that until $t = 200$ min, a fairly strong agreement between the numerical and experimental results is obtained. It corresponds to the constant rate settling phase and to the beginning of the hindered settling phase of the total process.

The results show that by an appropriate choice of the particle diameter (corresponding to the mean diameter) it is possible to fit quite well the experimental results during the settling phase. Obviously it is more difficult to simulate the hindered settling and the consolidation processes with the actual assumptions (the flocculation and deflocculating processes are not account for).

The conclusion of this test is that the actual model is able to represent reasonably the fine-grained suspended-sediment transport in an estuary but not the very concentrated sediment bed evolution. Future research will concern the development of the flocculation and the consolidation modelling in the frame of the two-phase flow approach.

4. Application to the Seine estuary (France)

An attempt has been made to simulate the suspended-sediment transport in a real estuary, the Seine estuary, in order to illustrate the feasibility of the present model. The Seine estuary extends over about 160 km from the mouth to the Dam of Poses (Fig. 6). It is a macro-tidal and hyposynchronic estuary with mean tidal ranges of about 7 m. The annual mean river flow is nearly 500 $m^3\ s^{-1}$, with lowest and highest values of 100 and 2000 $m^3\ s^{-1}$, respectively. A turbidity of about 2 $g\ l^{-1}$ is frequently observed in the TM.

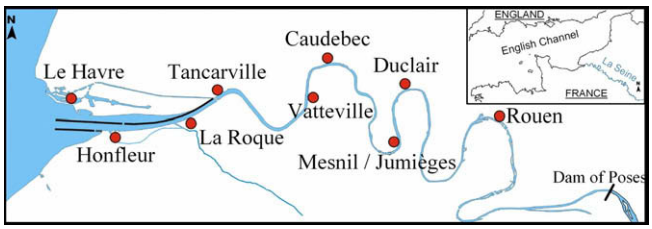

Fig. 6. Location of the computed domain for the Seine estuary.

The Seine estuary, the bathymetry of which has been extracted from the SHOM (Service Hydrographique et Océanographique de la Marine, France) map, is discretised by a computing mesh of 320 longitudinal points and 31 vertical points with refinement near the bottom and near the mouth.

The tidal conditions are imposed at the sea boundary. A river flow of 300 $m^3\ s^{-1}$, corresponding to a low discharge period, is specified at the upstream boundary. No solid discharge is set at the inland boundary, i.e. the water is clear, and $\alpha_s = 0$. Initially, a stock of sediment of 16 μm diameter is positioned as a 100 cm thick layer at a distance of 45 km between La Roque and Caudebec. This represents a sediment stock of 650,000 tones. The simulations have been performed for a half moon cycle (14 days).

It is necessary to note that the computing domain could not be extended into the English Channel and does not cover the Seine bay, in which there are sediment exchanges with the Seine estuary. A 2-D horizontal model for sediment transport in the Seine Bay could be proposed and eventually coupled with the present model to obtain the boundary conditions for sediment fluxes coming from the sea. However, it currently lies beyond the scope of this study. A virtual reservoir is therefore introduced into the model to allow these exchanges to be taken into account. Initially, this reservoir is empty, but over time it is filled by the sediment fluxes flowing out of the estuary. For inflow, the solid fraction at the sea boundary will be calculated by the ratio of the mass of sediment in the reservoir over the total water volume, flowing out during the previous ebb period. While such conditions may leave the model open to criticism, they do ensure total mass conservation in the model. A mixed length model is used to simulate the fluid phase turbulence in which the mixing length is modelled by the formulation of Escudier [39].

Water levels and mean current velocity are compared with measures of the SHOM for spring and neap tide at different stations along the Seine (Fig. 7). The curve of water levels is almost sinusoid at Honfleur (8 km from the river mouth) and becomes asymmetric at Duclair (87 km from the river mouth). The flood lasts 4 h whereas it is 8 h for the ebb. This asymmetry can be observed in current velocity. As a consequence, current velocity during the flood is stronger than during the ebb. These strong currents are partially responsible for erosion of the river bed, a phenomenon called "tidal pumping" (Allen et al. [40]). In the Seine estuary, this process is of major import for sediment transport (Brenon and Le Hir [2]).

The tidal and river flow conditions used here are closed to those used by SAUM (SAUM – Schéma d'Aptitude et d'Utilisation de la Mer – see Avoine et al. [41]). It has been observed that in neap tide and at low river flow, the quantity of suspended matter is low and the turbidity is about 0.2 g l^{-1} (Avoine [42]). The TM has clearly not been reached. Similarly, the numerical model predicts a low quantity of suspended matter in neap tide, of about 0.1 g l^{-1} near Honfleur, where the TM is not detected by the model either.

Fig. 8 shows the numerical results and observations in spring tide. The observations show that the TM developed over the entire water depth at Low Water Levels (LWL) and a strong decantation at High Water Levels (HWL). The observed concentration could reach more than 1 g l^{-1}. The TM moves over the longitudinal distance between Honfleur and Tancarville during a tidal cycle. The numerical model predicts a TM obviously formed with a maximal concentration of about 1 g l^{-1}. Its core is located at 8 km from the river mouth, near Honfleur, at LWL and at 20 km, near Tancarville, at HWL. This corresponds to a horizontal displacement of 12 km as observed during a tidal cycle. However in comparison with the observations, the TM reproduced by the present model is not enough developed on the vertical. Indeed, at LW moment the model predicts a concentration of less than 0.1 g l^{-1} in the upper half depth whereas the observations show a TM fully developed over the entire water depth with a concentration of more than 1.0 g l^{-1}. Similarly, at HWL the concentration observed in the bottom half depth is about 1.0 g l^{-1} over a distance of 18 km while the calculated concentration in the same layer is below 0.1 g l^{-1} (see Fig. 8). This is explained by the fact that the hindering process is not correctly simulated by the model, thus the solid particles are not sufficiently maintained in suspension. This default should be corrected in the future development.

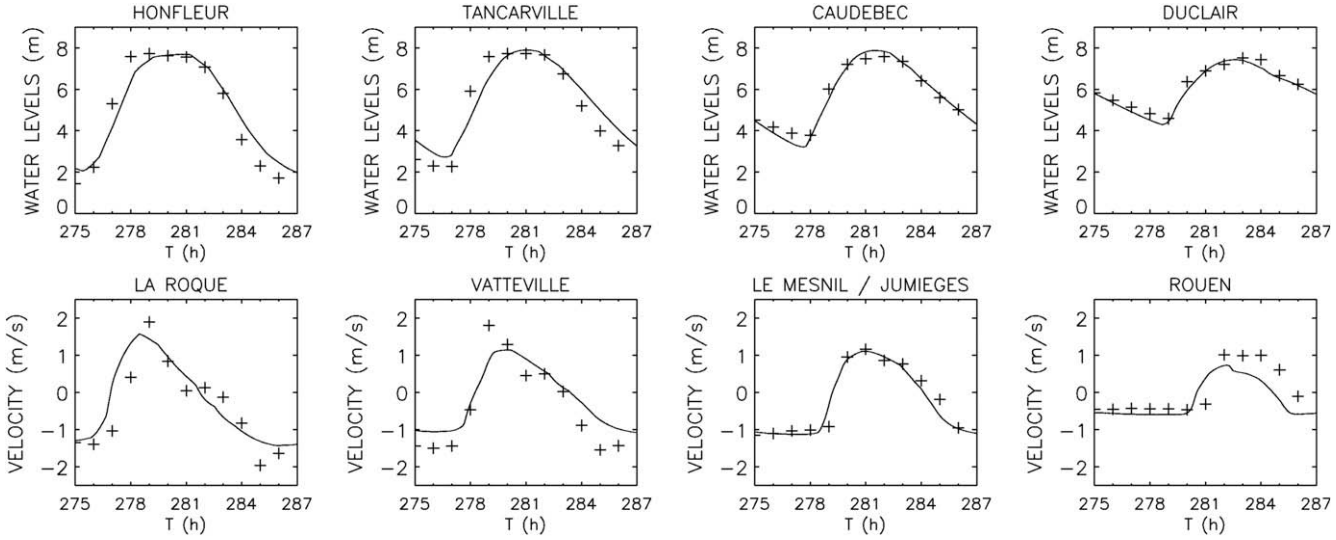

Fig. 7. Calibration results in spring tide: computational (–); measured (+).

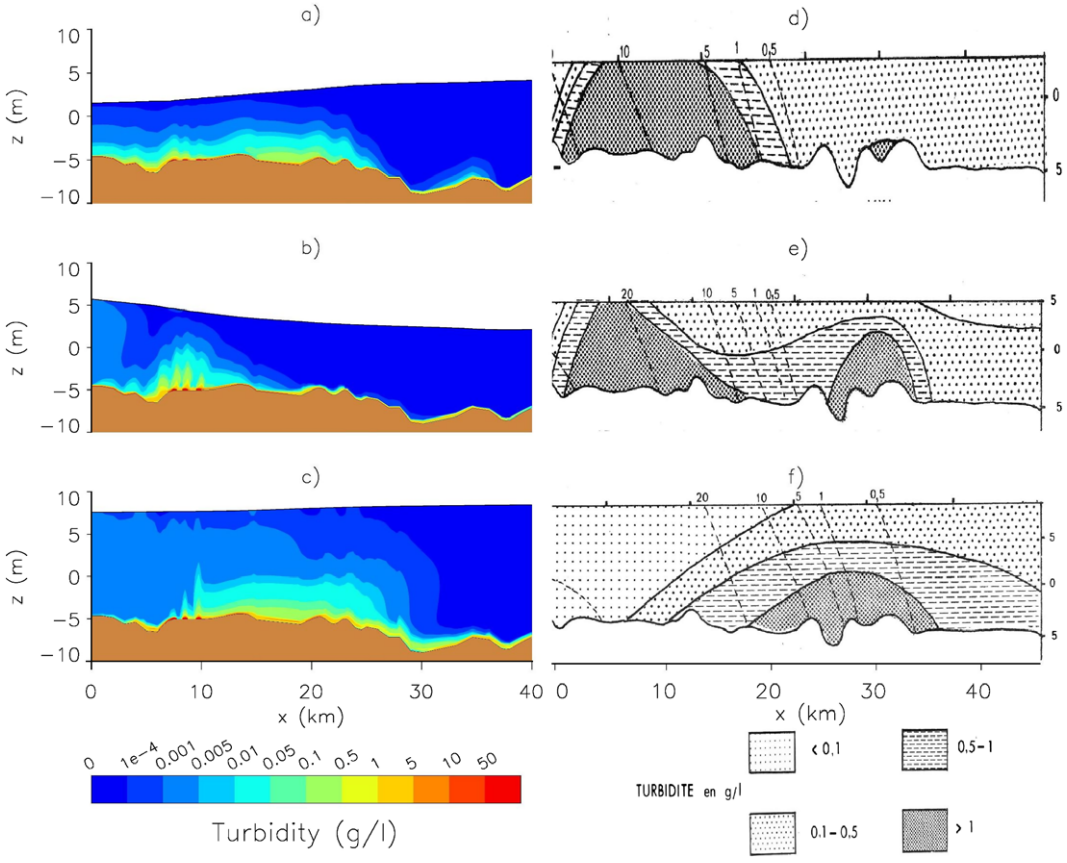

Fig. 8. Contour map of turbidity in spring tide from the two-phase model (left) and from the observations: (a) at LW; (b) LW+3; and (c) HW.

Although the quantitative agreement between the numerical results and the observations is not satisfying yet, the main characteristics of estuarine hydro-sediment dynamics of the Seine estuary have been reproduced by the proposed model. Moreover, the formation and displacement of the computed TM in the Seine estuary are in an overall agreement with the observed results. The results demonstrate the acceptable behavior of the model for the suspended-sediment transport in a real estuary in different tidal conditions. One of the benefits of a two-phase model resides in the treatment of the river bed. The fluid-mud layer moves horizontally, under the influence of tidal currents and river flows and serves as a solid-particle reservoir for the TM. This cannot be described in a classic sediment transport model which in itself illustrates one of the major attractions of a two-phase model. At present, such a model requires considerable CPU time: 33 h CPU on a PC of 2.66 GHz for a 14 day simulation.

5. Conclusions and perspectives

A full 2-D X/Z two-phase model based on the theory of granular flows has been developed and presented above for the simulation of sediment transport in estuaries. As this model takes into consideration the fluid–solid particles and particle–particle interactions, it could reproduce the sedimentation processes such as described in test-cases 3.1 and 3.2, which no single-phase model can simulate. Additionally, the numerical results, when quantitatively compared with the experimental data, illustrate the accurate behavior of the model in describing the transport and the sedimentation of non-cohesive particles even in very dense, particle-laden flows ($\alpha_s > 0.48$). However, the flocculating and deflocculating processes are yet to be taken into consideration. This is an area of research which could further improve the capacity of the model to accurately simulate cohesive-sediment transport. The Seine estuary application shows that the model allows us to overcome the major difficulties met in modelling sediment transport in estuaries: (i) the computed domain extends from the true and non-erodible bottom; (ii) no empiric formula is needed to calculate the deposit and erosion fluxes These sediment exchange fluxes are calculated inside the model. Cleary, the Seine estuary application shows encouraging results of the model for simulating suspended-sediment transport in a real estuary.

Future research will focus on flocculation processes, and turbulence modelling that are important in the frame of estuarine applications. Note that some work concerning two-phase flow turbulence modelling for sediment transport models was conducted by Chauchat and Guillou [24]. This work concerns small scale laboratory experiments and gives a strong improvement compared to classical sediment transport models. But more work has to be done on turbulence modelling at estuaries scale.

Acknowledgement

Miss N. Barbry [43] enjoyed the financial support of the European Commission (FP4-Contract ERBIC18CT960111-Cuu-Long Project), of the Regional Council of the Lower-Normandy and the "Agence de l'Eau de Normandie". Mr Julien Chauchat [44] was financially supported by the European Commission (the FLOCODS Project, FP5-Contract No. ICA4-CT2001-10035) and by CETMEF (Centre d'Etude Technique Maritime Et Fluviale, French Ministry of Equipment and Transport).

Appendix A. Governing equations

- For the fluid phase:

Continuity equation:

$$\frac{\partial \alpha_f}{\partial t^*} - \frac{1}{HB}\sigma\frac{\partial \eta}{\partial t^*}\frac{\partial \alpha_f B}{\partial \sigma} + \frac{1}{B}\left(\frac{\partial(\alpha_f B u_f)}{\partial x^*} + \omega_1\frac{\partial(\alpha_f B u_f)}{\partial \sigma} + \frac{1}{H}\frac{\partial(\alpha_f B w_f)}{\partial \sigma}\right) = 0 \quad (A.1)$$

where u, w are the velocity components in x- and z-direction, respectively.
Momentum equation:
In x-direction:

$$\frac{\partial u_f}{\partial t^*} + u_f\frac{\partial u_f}{\partial x^*} + \omega\frac{\partial u_f}{\partial \sigma} = -\frac{1}{\rho_f}\left(\frac{\partial p_f}{\partial x^*} + \omega_1\frac{\partial p_f}{\partial \sigma}\right) + \frac{C_D}{\rho_f \alpha_f}(u_f - u_s) - \frac{1}{4\alpha_f}|\vec{u}_f - \vec{u}_s|^2\left(\frac{\partial \alpha_f}{\partial x^*} + \omega_1\frac{\partial \alpha_f}{\partial \sigma}\right) - \frac{\beta \nu_f}{\alpha_f}T_1 + \frac{1}{\alpha_f B}(T_2 + T_3) \quad (A.2)$$

In z-direction:

$$\frac{\partial w_f}{\partial t^*} + u_f\frac{\partial w_f}{\partial x^*} + \omega\frac{\partial w_f}{\partial \sigma} = -\frac{1}{\rho_f}\frac{1}{H}\frac{\partial p_f}{\partial \sigma} - g + \frac{C_D}{\rho_f \alpha_f}(w_f - w_s) - \frac{1}{4\alpha_f}|\vec{u}_f - \vec{u}_s|^2\frac{1}{H}\frac{\partial \alpha_f}{\partial \sigma} - \frac{\beta \nu_f}{\alpha_f}T_4 + \frac{1}{\alpha_f B}(T_5 + T_6) \quad (A.3)$$

where

$$\omega = \frac{1}{H}\left[w_f + u_f\left(\frac{\partial h}{\partial x^*} - \sigma\frac{\partial H}{\partial x^*}\right) - \sigma\frac{\partial \eta}{\partial t^*}\right]: \quad \text{and}$$

$$\omega_1 = \frac{1}{H}\left(\frac{\partial h}{\partial x^*} - \sigma\frac{\partial H}{\partial x^*}\right)$$

$$T_1 = 2\left(\frac{\partial \alpha_f}{\partial x^*} + \omega_1\frac{\partial \alpha_f}{\partial \sigma}\right)\left(\frac{\partial u_f}{\partial x^*} + \omega_1\frac{\partial u_f}{\partial \sigma}\right) + \frac{1}{H}\frac{\partial \alpha_f}{\partial \sigma}\left[\frac{1}{H}\frac{\partial u_f}{\partial \sigma} + \left(\frac{\partial w_f}{\partial x^*} + \omega_1\frac{\partial w_f}{\partial \sigma}\right)\right]$$

$$T_2 = \frac{\partial}{\partial x^*}\left[\alpha_s \nu_f\left(\frac{\partial u_s B}{\partial x^*} + \omega_1\frac{\partial u_s B}{\partial \sigma}\right)\right] + \omega_1\frac{\partial}{\partial \sigma}\left[\alpha_s \nu_f\left(\frac{\partial u_s B}{\partial x^*} + \omega_1\frac{\partial u_s B}{\partial \sigma}\right)\right] + \frac{1}{H^2}\frac{\partial}{\partial \sigma}\left(\frac{\alpha_s \nu_f}{2}\frac{\partial u_s B}{\partial \sigma}\right) + \frac{1}{H}\frac{\partial}{\partial \sigma}\left[\frac{\alpha_s \nu_f}{2}\left(\frac{\partial w_s B}{\partial x^*} + \omega_1\frac{\partial w_s B}{\partial \sigma}\right)\right]$$

$$T_3 = \frac{\partial}{\partial x^*}\left[\alpha_f \nu_f\left(\frac{\partial u_f B}{\partial x^*} + \omega_1\frac{\partial u_f B}{\partial \sigma}\right)\right] + \omega_1\frac{\partial}{\partial \sigma}\left[\alpha_f \nu_f\left(\frac{\partial u_f B}{\partial x^*} + \omega_1\frac{\partial u_f B}{\partial \sigma}\right)\right] + \frac{1}{H}\frac{\partial}{\partial \sigma}\left[\frac{\alpha_f \nu_f}{2}\left(\frac{1}{H}\frac{\partial u_f B}{\partial \sigma} + \frac{\partial w_f B}{\partial x^*} + \omega_1\frac{\partial w_f B}{\partial \sigma}\right)\right]$$

$$T_4 = \left(\frac{\partial \alpha_f}{\partial x^*} + \omega_1\frac{\partial \alpha_f}{\partial \sigma}\right)\left(\frac{1}{H}\frac{\partial u_f}{\partial \sigma} + \frac{\partial w_f}{\partial x^*} + \omega_1\frac{\partial w_f}{\partial \sigma}\right) + \frac{2}{H^2}\frac{\partial \alpha_f}{\partial \sigma}\frac{\partial w_f}{\partial \sigma}$$

$$T_5 = \frac{\partial}{\partial x^*}\left[\frac{\alpha_s \nu_f}{2}\left(\frac{1}{H}\frac{\partial u_s B}{\partial \sigma} + \frac{\partial w_s B}{\partial x^*} + \omega_1\frac{\partial w_s B}{\partial \sigma}\right)\right] + \omega_1\frac{\partial}{\partial \sigma}\left[\frac{\alpha_s \nu_f}{2}\left(\frac{1}{H}\frac{\partial u_s B}{\partial \sigma} + \frac{\partial w_s B}{\partial x^*} + \omega_1\frac{\partial w_s B}{\partial \sigma}\right)\right] + \frac{1}{H^2}\frac{\partial}{\partial \sigma}\left(\alpha_s \nu_f\frac{\partial w_s B}{\partial \sigma}\right)$$

$$T_6 = \frac{\partial}{\partial x^*}\left[\frac{\alpha_f \nu_f}{2}\left(\frac{\partial u_f B}{\partial x^*} + \omega_1\frac{\partial u_f B}{\partial \sigma} + \frac{1}{H}\frac{\partial w_f B}{\partial \sigma}\right)\right] + \omega_1\frac{\partial}{\partial \sigma}\left[\frac{\alpha_f \nu_f}{2}\left(\frac{\partial u_f B}{\partial x^*} + \omega_1\frac{\partial u_f B}{\partial \sigma} + \frac{1}{H}\frac{\partial w_f B}{\partial \sigma}\right)\right] + \frac{1}{H^2}\frac{\partial}{\partial \sigma}\left(\alpha_f \nu_f\frac{\partial w_f B}{\partial \sigma}\right)$$

- For the solid phase:

Continuity equation:

$$\frac{\partial \alpha_s}{\partial t^*} - \frac{1}{HB}\sigma\frac{\partial \eta}{\partial t^*}\frac{\partial \alpha_s B}{\partial \sigma} + \frac{1}{B}\left(\frac{\partial(\alpha_s B u_s)}{\partial x^*} + \omega_1\frac{\partial(\alpha_s B u_s)}{\partial \sigma} + \frac{1}{H}\frac{\partial(\alpha_s B w_s)}{\partial \sigma}\right) = 0 \quad (A.4)$$

Momentum equation:
In x-direction:

$$\frac{\partial u_s}{\partial t^*} + u_s\frac{\partial u_s}{\partial x^*} + \omega\frac{\partial u_f}{\partial \sigma} = -\frac{1}{\rho_s}\left(\frac{\partial p_s}{\partial x^*} + \omega_1\frac{\partial p_s}{\partial \sigma}\right) + \frac{C_D}{\rho_s \alpha_s}(u_f - u_s) - \frac{\beta \mu_f}{\rho_s \alpha_s}T_7 + \frac{1}{\rho_s \alpha_s B}(T_8 + T_9) \quad (A.5)$$

In z-direction:

$$\frac{\partial w_s}{\partial t^*} + u_s\frac{\partial w_s}{\partial x^*} + \omega\frac{\partial w_s}{\partial \sigma} = -\frac{1}{\rho_s}\frac{1}{H}\frac{\partial p_s}{\partial \sigma} - g + \frac{C_D}{\rho_s \alpha_s}(w_f - w_s) - \frac{\beta \mu_f}{\rho_s \alpha_s}T_{10} + \frac{1}{\rho_s \alpha_s B}(T_{11} + T_{12}) \quad (A.6)$$

where

$$T_7 = 2\left(\frac{\partial \alpha_s}{\partial x^*} + \omega_1\frac{\partial \alpha_s}{\partial \sigma}\right)\left(\frac{\partial u_f}{\partial x^*} + \omega_1\frac{\partial u_f}{\partial \sigma}\right) + \frac{1}{H}\frac{\partial \alpha_s}{\partial \sigma}\left[\frac{1}{H}\frac{\partial u_f}{\partial \sigma} + \left(\frac{\partial w_f}{\partial x^*} + \omega_1\frac{\partial w_f}{\partial \sigma}\right)\right]$$

$$T_8 = \frac{\partial}{\partial x^*}\left[\alpha_s^2 \beta \mu_f\left(\frac{\partial u_s B}{\partial x^*} + \omega_1\frac{\partial u_s B}{\partial \sigma}\right)\right] + \omega_1\frac{\partial}{\partial \sigma}\left[\alpha_s^2 \beta \mu_f\left(\frac{\partial u_s B}{\partial x^*} + \omega_1\frac{\partial u_s B}{\partial \sigma}\right)\right] + \frac{1}{H^2}\frac{\partial}{\partial \sigma}\left(\frac{\alpha_s^2 \beta \mu_f}{2}\frac{\partial u_s B}{\partial \sigma}\right) + \frac{1}{H}\frac{\partial}{\partial \sigma}\left[\frac{\alpha_s^2 \beta \mu_f}{2}\left(\frac{\partial w_s B}{\partial x^*} + \omega_1\frac{\partial w_s B}{\partial \sigma}\right)\right]$$

$$T_9 = \frac{\partial}{\partial x^*}\left[\alpha_f \alpha_s \beta \mu_f\left(\frac{\partial u_f B}{\partial x^*} + \omega_1\frac{\partial u_f B}{\partial \sigma}\right)\right] + \omega_1\frac{\partial}{\partial \sigma}\left[\alpha_f \alpha_s \beta \mu_f\left(\frac{\partial u_f B}{\partial x^*} + \omega_1\frac{\partial u_f B}{\partial \sigma}\right)\right] + \frac{1}{H}\frac{\partial}{\partial \sigma}\left[\frac{\alpha_f \alpha_s \beta \mu_f}{2}\left(\frac{1}{H}\frac{\partial u_f B}{\partial \sigma} + \frac{\partial w_f B}{\partial x^*} + \omega_1\frac{\partial w_f B}{\partial \sigma}\right)\right]$$

$$T_{10} = \left(\frac{\partial \alpha_s}{\partial x^*} + \omega_1\frac{\partial \alpha_s}{\partial \sigma}\right)\left(\frac{1}{H}\frac{\partial u_f}{\partial \sigma} + \frac{\partial w_f}{\partial x^*} + \omega_1\frac{\partial w_f}{\partial \sigma}\right) + \frac{2}{H^2}\frac{\partial \alpha_s}{\partial \sigma}\frac{\partial w_f}{\partial \sigma}$$

$$T_{11}=\frac{\partial}{\partial x^*}\left[\frac{\alpha_s^2\beta\mu_f}{2}\left(\frac{1}{H}\frac{\partial u_sB}{\partial\sigma}+\frac{\partial w_sB}{\partial x^*}+\omega_1\frac{\partial w_sB}{\partial\sigma}\right)\right]+\omega_1\frac{\partial}{\partial\sigma}\left[\frac{\alpha_s^2\beta\mu_f}{2}\left(\frac{1}{H}\frac{\partial u_sB}{\partial\sigma}+\frac{\partial w_sB}{\partial x^*}+\omega_1\frac{\partial w_sB}{\partial\sigma}\right)\right]+\frac{1}{H^2}\frac{\partial}{\partial\sigma}\left(\alpha_s^2\beta\mu_f\frac{\partial w_sB}{\partial\sigma}\right)$$

$$T_{12}=\frac{\partial}{\partial x^*}\left[\frac{\alpha_s\alpha_f\beta\mu_f}{2}\left(\frac{\partial u_fB}{\partial x^*}+\omega_1\frac{\partial u_fB}{\partial\sigma}+\frac{1}{H}\frac{\partial w_fB}{\partial\sigma}\right)\right]+\omega_1\frac{\partial}{\partial\sigma}\left[\frac{\alpha_s\alpha_f\beta\mu_f}{2}\left(\frac{\partial u_fB}{\partial x^*}+\omega_1\frac{\partial u_fB}{\partial\sigma}+\frac{1}{H}\frac{\partial w_fB}{\partial\sigma}\right)\right]+\frac{1}{H^2}\frac{\partial}{\partial\sigma}\left(\alpha_s\alpha_f\beta\mu_f\frac{\partial w_fB}{\partial\sigma}\right)$$

Appendix B. Boundary conditions

- On the surface, two conditions are imposed as follows
  (i) Dynamic condition: the fluid pressure on the free surface, $p_{f,z=\eta}$ should be equal to the atmospheric pressure,

$$p_{atm}: p_{f,z=\eta}=p_{atm}. \tag{B.7a}$$

  (ii) Kinematic condition:

$$\frac{\partial\eta}{\partial t}+u_\eta\frac{\partial\eta}{\partial x}=w_\eta \tag{B.7b}$$

  where $\begin{cases}u_\eta=(\alpha_f u_{\eta,f}+\alpha_s u_{\eta,s})\\ w_\eta=(\alpha_f w_{\eta,f}+\alpha_s w_{\eta,s})\end{cases}$ are the velocity components on the free surface in x- and z-direction, respectively. This condition is replaced by $\frac{\partial\eta}{\partial t}+\frac{\partial Q_m}{\partial x}=w_\eta$, where $Q_m=\int_{-h}^{\eta}u_mBdz$ represents the horizontal volume flux of fluid-particles mixture.
- On the bottom, the non-slip condition for velocity $u_{z=-h}=(\alpha_f u_f+\alpha_s u_s)_{z=-h}=0$ and $w_{z=-h}=(\alpha_f w_f+\alpha_s w_s)_{z=-h}=0$, and the reflection condition for the pressure $\frac{\partial p_f^+}{\partial z}=-\rho_f g$ are imposed.

Appendix C. Chorin's technique

Eqs. (A.1)–(A.3) for the fluid phase are resolved in two successive steps:

– Convection and diffusion step:

$$\begin{cases}\frac{u_f^+-u_f^n}{\Delta t^*}+u_f\frac{\partial u_f}{\partial x^*}+\omega\frac{\partial u_f}{\partial\sigma}=-\frac{1}{\rho_f}\left(\frac{\partial p_f^+}{\partial x^*}+\omega_1\frac{\partial p_f^+}{\partial\sigma}\right)\\ +\frac{C_D}{\rho_f\alpha_f}(u_f-u_s)-\frac{1}{4\alpha_f}|\vec{u}_f-\vec{u}_s|^2\left(\frac{\partial\alpha_f}{\partial x^*}+\omega_1\frac{\partial\alpha_f}{\partial\sigma}\right)\\ -\frac{\beta\nu_f}{\alpha_f}T_1+\frac{1}{\alpha_fB}(T_2+T_3)\frac{w_f^+-w_f^n}{\Delta t^*}+u_f\frac{\partial w_f}{\partial x^*}+\omega\frac{\partial w_f}{\partial\sigma}=-\frac{1}{\rho_f}\frac{1}{H}\frac{\partial p_f^+}{\partial\sigma}\\ -g+\frac{C_D}{\rho_f\alpha_f}(w_f-w_s)-\frac{1}{4\alpha_f}|\vec{u}_f-\vec{u}_s|^2\frac{1}{H}\frac{\partial\alpha_f}{\partial\sigma}\\ -\frac{\beta\nu_f}{\alpha_f}T_4+\frac{1}{\alpha_fB}(T_5+T_6)\end{cases} \tag{C.8}$$

– Pressure step:

$$\begin{cases}\frac{\alpha_f^{n+1}-\alpha_f^n}{\Delta t^*}-\frac{1}{HB}\sigma\frac{\partial\eta}{\partial t^*}\frac{\partial\alpha_fB}{\partial\sigma}\\ +\frac{1}{B}\left(\frac{\partial(\alpha_fBu_f^{n+1})}{\partial x^*}+\omega_1\frac{\partial(\alpha_fBu_f^{n+1})}{\partial\sigma}+\frac{1}{H}\frac{\partial(\alpha_fBw_f^{n+1})}{\partial\sigma}\right)=0\\ \frac{u_f^{n+1}-u_f^+}{\Delta t^*}=-\frac{1}{\rho_f}\left(\frac{\partial p_f^{n+1}-p_f^n}{\partial x^*}+\omega_1\frac{\partial p_f^{n+1}-p_f^n}{\partial\sigma}\right)\\ \frac{w_f^{n+1}-w_f^+}{\Delta t^*}=-\frac{1}{\rho_f}\frac{1}{H}\frac{\partial p_f^{n+1}-p_f^n}{\partial\sigma}\end{cases} \tag{C.9}$$

In this step, the combination of three equations of (A.9) allows us to establish the equation for an only unknown that is the fluid pressure:

$$\begin{aligned}&\frac{\partial}{\partial x^*}\left(\alpha_fB\left(\frac{\partial dp_f}{\partial x^*}+\omega_1\frac{\partial dp_f^n}{\partial\sigma}\right)\right)+\omega_1\frac{\partial}{\partial\sigma}\left(\alpha_fB\left(\frac{\partial dp_f}{\partial x^*}+\omega_1\frac{\partial dp_f^n}{\partial\sigma}\right)\right)\\ &\quad+\frac{1}{H}\frac{\partial}{\partial\sigma}\left(\alpha_fB\frac{1}{H}\frac{\partial dp_f}{\partial\sigma}\right)\\ &=\frac{\rho_f}{\Delta t^*}\left(\frac{\partial(\alpha_fBu_f^+)}{\partial x^*}+\omega_1\frac{\partial(\alpha_fBu_f^+)}{\partial\sigma}+\frac{1}{H}\frac{\partial(\alpha_fBw_f^+)}{\partial\sigma}\right)\\ &\quad+\frac{\rho_fB}{\Delta t^*}\frac{\alpha_f^{n+1}-\alpha_f^n}{\Delta t^*}-\frac{\rho_f}{\Delta t^*}\frac{1}{H}\sigma\frac{\partial\eta}{\partial t^*}\frac{\partial\alpha_fB}{\partial\sigma}\end{aligned} \tag{C.10}$$

where $dp_f=p_f^{n+1}-p_f^n$.

References

[1] Blaas M, Dong C, Marchesiello P, McWilliams JC, Stolzenbach KD. Sediment-transport modelling on Southern Californian shelves: A ROMS case study. Cont Shelf Res 2007;27:832–53.
[2] Brenon I, Le Hir P. Simulation du bouchon vaseux dans l'estuaire de la Seine: capacité et limites d'un modèle bidimensionnel horizontal. CR Acad Sci (série II A) 1999;332:327–8.
[3] Gleinzon P, Punt A-G, Lyons M-G. Modelling hydrodynamics and sediment flux within a macro-tidal estuary: problems and solutions. Sci Total Environ 2003;314–316:589–97.
[4] Li ZH, Nguyen KD, Brun-Cottan JC, Martin JM. Numerical simulation of Saline intrusion and suspended matter transport in the Gironde Estuary by a 2-D width-integrated model. Oceanol Acta 1994;17(5):479–500.
[5] Liu W-C, Hsu M-H, Kuo A-Y. Modelling of hydrodynamics and cohesive sediment transport in Tanshui River estuarine system, Taiwan. Marine Pollut Bull 2002;44:1076–88.
[6] Lopes JF, Dias JM, Dekeyser I. Numerical modelling of cohesive sediment transport in the Ria de Aveiro Lagoon, Portugal. J Hydrol 2006;319:176–98.
[7] Lumborg U. Modelling the deposition, erosion, and flux of cohesive sediment through Oresund. J Marine Syst 2005;56:179–93.
[8] Lumborg U, Pejrup M. Modelling of cohesive sediment transport in a Tidal Lagoon – an annual budget. Marine Geol 2005;218:1–16.
[9] Nguyen KD, Phan NV, Guillou S. A 3-D numerical study for the saline intrusion and the sediment transport in the Gironde Estuary (France). Renmin Zhujiang 2007;158:27–34.
[10] Peng J, Zeng EY. An integrated geochemical and hydrodynamic model for Tidal coastal environments. Marine Chem 2007;103:15–29.
[11] Rolinski S, Umgiesser G. Modelling short-term dynamics of suspended particulate matter in Venice Lagoon, Italy, Estuarine. Coastal Shelf Sci 2005;63:561–76.
[12] Winterwerp JC, Van Kesteren WG. Introduction to the physics of cohesive sediment in the marine environment. Elsevier; 2004. 576 p.
[13] Mehta AJ, Parchure T, Dixit JG, Ariathurai R. Resuspension potential of deposited cohesive beds. In: Kenedy V, editor. Estuarine comparison. Academic Press; 1982. p. 591–609.
[14] Ariathurai CR, Arulanandan K. Erosion rates of cohesive soils. J Hydraul Div: Proc Am Soc Civil Eng 1978;104(HY2):279–83.
[15] Partheniades E. Erosion and deposition of cohesive soils. J Hydraul Div Proc ASCE 1965;91(HY1):105–39.
[16] Hayter EJ, Mehta AJ. Modelling cohesive sediments transport in estuarine waters. Appl Math Modell 1986;10(4):294–303.
[17] Krone RB. Flume studies of the transport of sediment in estuarial processes. Final Report, Hydraulic Engineering Laboratory and Sanitary Engineering Research Laboratory, University of California, Berkeley; 1962.
[18] Teisson C, Simonin O, Galland JC, Laurence D. Turbulence and mud sedimentation: a Reynolds stress model and a two-phase flow model. In: Proceedings of 23rd international conference on coastal engineering, ASCE; 1992. p. 2853–66.
[19] Simonin O. Prediction of the dispersed phase turbulence in particule-laden jets. Gas–Solid Flows ASME–FED 1991;121:197–206.
[20] Vilaret C, Davies AG. Modelling of sediment–turbulent flow interactions. Appl Mech Rev 1995;48:601–9.
[21] Greimann BP, Holly FM. Two-phase flow analysis of concentration profiles. ASCE J Hydraul Eng 2001;127(9):753–62.
[22] Barbry N, Guillou S, Nguyen KD. Une approche diphasique pour le calcul du transport sédimentaire en milieux estuariens. CR Acad Sci série II B 2000;328:793–9.
[23] Guillou S, Barbry N, Nguyen KD. Calcul numérique des ondes de surface par une méthode de projection et un maillage eulérien adaptatif. CR Acad Sci (série II B) 2000;328:875–81.
[24] Chauchat J, Guillou S. On turbulence closures for two-phase sediment-laden flows models. J Geophys Res 2008;113:C11017. doi:10.1029/2007JC004708.

[25] Drew DA, Lahey RT. Analytical modelling of multiphase flow. In: Roco MC, editor. Particulate two-phase flow. Boston: Butterworth–Heinemann; 1993.
[26] Lundgren TS. Slow flow through stationary random beds and suspensions of spheres. J Fluid Mech 1972;51:273–99.
[27] Einstein A. Eine Neue Bestimmung der Molekuldimensionen. Ann Phys 1906;19:289–306.
[28] Graham AL. On the viscosity of suspensions of solid spheres. Appl Sci Res 1981;37:275–86.
[29] Enwald H, Peirano E, Almstedt AE. Eulerian two-phase flow theory applied to fluidisation. Int J Multiphase Flow 1996;22:21–66.
[30] Massoudi M, Rajagopal KR, Ekmann JM, Mathur MP. Remarks on the modeling of fluidised systems. AIChE J 1992;38:471–2.
[31] Peirano E, Leckner B. Fundamentals of turbulent gas–solid flows applied to circulating fluidized bed combustion. Prog Energy Combust Sci 1998;24:259–96.
[32] Deutsch E, Simonin O. Large Eddy simulation applied to the motion of particles in stationary homogeneous fluid turbulence. Turbulence Modification in Multiphase Flows ASME–FED 1991;110:35–42.
[33] Haider A, Levenspiel O. Drag coefficient and terminal velocity of spherical and non-spherical particles. Powder Technol 1989;58:63–70.
[34] Chorin AJ. Numerical solution of the Navier–Stokes equations. Math Comp 1968;22:745–62.
[35] Guillou S, Nguyen KD. An improved technique for solving the two-dimensional shallow-water problems. Int J Numer Methods Fluids 1999;29(4):465–83.
[36] Pham Van Bang D, Lefrançois E, Ovarlez G, Bertrand F. Mri experimental and 1d fe–fct numerical investigation of the sedimentation and consolidation. In: Seventh international conference on hydroinformatics; 2006.
[37] Hsu T, Jenkins JT, Liu LF. On two-phases diment transport: dilute flow. J Geophys Res 2003;108:14.
[38] Rouas G. Etude et Modélisation par éléments finis des processus hydrosédimentaires et estuariens, Ph.D. thesis, Université de Technologie de Compiègne; 1996.
[39] Escudier MP. The distribution of mixing length in turbulent flow near walls. Heat transfer section report TWF/TN/1, Imperial College; 1966.
[40] Allen GP, Salomon JC, Bassoulet P, Du Penhoat Y, Dé Grandpré C. Effects of tides on mixing and suspended-sediment transport in macro-tidal estuaries. Sediment Geol 1980;26:69–90.
[41] Avoine J, Dupont JP, David F. Etudes hydrosédimentaires, étude des suspensions, programme géochimie, analyses par activation neutronique. Tech. report of University of Caen; 1980.
[42] Avoine J. L'estuaire de la Seine: sédiments et dynamique sédimentaire. PhD thesis, Université de Caen; 1981.
[43] Barbry N. Numerical modelling two-dimensional vertical X/Z of sediment transport in estuaries by a two-phase approach, Ph.D. thesis, University of Caen, France; 2000.
[44] Chauchat J. Contribution to the two-phase modelling for sediment transports in estuaries and coastal zones, Ph.D. thesis, University of Caen, France; 2007. <http://tel.archives-ouvertes.fr/tel-00173387/en/>.